Math. Model. Nat. Phenom. 13 (2018) 53
https://doi.org/10.1051/mmnp/2018079

Mathematical Modelling of Natural Phenomena
www.mmnp-journal.org

STUDY OF INTERNAL FLAME FRONT STRUCTURE OF ACCELERATING HYDROGEN/OXYGEN FLAMES WITH DETAILED CHEMICAL KINETICS AND DIFFUSION MODELS[☆]

V. Bykov and A. Koksharov[*]

Abstract. The problem of Detonation to Deflagration (DDT) is revisited. A stoichiometric hydrogen/oxygen combustion system is considered. The study focuses on the investigation of the system solution in the thermo-chemical state space of the system. The Σ model is implemented to study the flame acceleration and DDT in 1D formulation. The model was suggested to take into account wrinkling of the flame surface. In this way, the problem becomes treatable numerically even with the detailed mechanism of chemical kinetics and with detailed models for molecular diffusion. In order to treat and integrate the model a recently developed numerical scheme to deal with very stiff systems both in time and in space is introduced and applied. Typical system solution profiles of the ignition, quasi-deflagration, flame acceleration, DDT and detonation stages are considered to study the structure of the flame front in the system thermo-chemical state space. The results of computations show that at the stages of the ignition, deflagration and acceleration the flame structure in the state/composition space moderately depends on Σ, however, significant influence shows up during later stages of the flame acceleration and DDT. Moreover, the path of the solution in the detonation regime significantly deviates from that of deflagration. This means that accurate and quantitative study of the DDT is not possible without reliable mechanisms of chemical kinetics able to describe the system state space during the transient.

Mathematics Subject Classification. 80A25, 80A30.

Received April 19, 2018. Accepted December 19, 2018.

1. Introduction

The deflagration to detonation transition (DDT) is probably most complex problem in combustion. In order to treat the DDT quantitatively, all possible phenomena should be taken into account because hydrodynamical and combustion processes become extremely coupled having enormous differences in characteristic time and space scales. This makes the problem very difficult. In spite a considerable progress in understanding of combustion processes has been made in the past and recently, the problem remains open.

The problem is very important for applications and for safety issues. On one hand uncontrolled detonation is a very destructive phenomenon and it is important in risk assessment [34]. The detonation can be accounted

[☆] This work was supported by DFG grants no BY 94/2-1 and by RFFR grant no 17-53-12018.

Keywords and phrases: Laminar flames, ignition and flame acceleration, DDT, chemical kinetics.

Karlsruhe Institute of Technology (KIT), Institute of Technical Thermodynamics, Engelbert-Arnold-Strasse 4, Building 10.91, 76131 Karlsruhe, Germany.

[*] Corresponding author: koksharov@kit.edu

Article published by EDP Sciences

© EDP Sciences, 2019

for engine knock and engine damage [46]. On the other hand controlled detonation offers a new perspective in propulsion, such as pulse detonation and rotation detonation engines, which promise higher thermal and exergetic efficiency [17, 30].

In study of the problem a central role plays the so-called mechanism of the DDT. In this respect there are two principle scenarios, the first is when a large energy deposition happens within a very short time, which is shorter than the acoustic time scale, a direct initiation of the detonation occurs in this case [12, 18, 39]. In a more interesting and general case the detonation occur after an unsteady deflagration stage of the flame acceleration [11, 29, 45].

At present there is no quantitative and predictive theory of the DDT of the second scenario. It means for a given geometry of a combustion system and mixture composition it is very difficult to predict whether the DDT occurs or not. In the literature the following main mechanisms are considered as a candidates for the flame acceleration and final DDT, namely,

1. Finger flames – a transition from finger to tulip flame [43] leads to a rapid increase of the flame surface ratio accelerating the flame;
2. Wall friction, hydraulic resistance (Sivashinsky [2, 5]) leading to momentum and energy losses – following ideas of Zel'dovich [45], the pressure increase in the flame induction zone governs the acceleration;
3. Delayed burning phenomena – secondary reaction in the product side pushes the flame forward driving the flame acceleration [3, 4];
4. Acoustic instabilities – again (similar to finger flames) the flame instabilities [6, 7] courses the flame surface growth and, in turn, accelerating the flame;
5. Turbulence and compression waves interaction – strong interaction of the reaction flame front and accumulating shock waves [40], see *e.g.* [35] for more details.

It is straightforward to assume that turbulence is driving force behind the transition [31]. The flame surface grows increasing the flame speed, which has positive feedback on the flame acceleration. In [20] the author links turbulence intensity with DDT based on gradient of chemical reactivity [44]. There is a number of numerical investigations [28, 35] supporting this theory. However, in this context the mechanism of turbulence initiation and sufficient flame acceleration remains open.

There are also experimental evidences [37] that the DDT is not likely to be attributed to the gradient mechanism of Zeldovich. In the absences of shock-wave interaction other weaker mechanism such as Darrieus-Landau, thermal-diffusive and Rayleigh-Taylor instabilities gain more importance for turbulence generation [13, 23, 26, 27, 36].

Keeping this in mind and also remembering that the DDT is a localized phenomenon motivate us to implement and to study the 1D Σ-model introduced in [10] and extensively studied in later works [14–16]. Within this approach the complex phenomenon of flame wrinkling can be still described with 1D formulation using flame folding factor Σ which represents the ratio of the total area of the wrinkled front to the area associated with its average radius. It is implemented as a simple amplification of the chemical source term by Σ^2. This framework provides an unique opportunity to investigate possible mechanisms of the DDT in a very simple yet informative representative setting.

In this work, in contrary to our prevision study [24], where the transition to the detonation is reported and investigated in detail, the focus is made on the properties of the transition relevant to the chemical kinetics and to internal structure of the accelerating flame. The method used to integrate system in time is outlined first. It allows us very detailed and highly resolved in time and in space computations needed to treat the problem. Next, the method is validated by using the structure of the stationary deflagration flame propagation problem. Afterwards, combustion system configuration for the DDT and numerical implementation are presented and discussed. Finally, the system transient unsteady behaviour is investigated in the system thermo-chemical state space. Additionally, the recently suggested global criteria of the DDT [21, 22] is tested locally to show the strength and accuracy of the numerical computation tool developed.

2. Mathematical model and numerical method

2.1. Mathematical model

In the current study, multicomponent Navier-Stokes equations with detailed hydrogen chemistry and species transport models are used. The flame wrinkling was adopted from [14, 16]. In physical units the set of governing equations reads then as follows (see also [41, 42]):
momentum

$$\frac{\partial}{\partial t}(\rho u) + \frac{\partial}{\partial x}\left(\rho u^2 + P - \frac{4}{3}\mu\frac{\partial u}{\partial x}\right) = 0, \tag{2.1}$$

energy

$$\frac{\partial}{\partial t}\left(\sum_i h_i c_i - P + \frac{1}{2}\rho u^2\right) + \frac{\partial}{\partial x}\left(u\left(\sum_i h_i c_i + \frac{1}{2}\rho u^2 - \frac{4}{3}\mu\frac{\partial u}{\partial x}\right) + \sum_k h_k\, j_k^d - \lambda\frac{\partial T}{\partial x}\right) = 0, \tag{2.2}$$

concentrations

$$\frac{\partial}{\partial t}(c_i) + \frac{\partial}{\partial x}\left(u c_i + j_i^d\right) = \Sigma^2\dot{\omega}_i, \quad i = 1, \ldots, n_s \tag{2.3}$$

state

$$P = R_0 T \sum_i c_i \tag{2.4}$$

density-concentration relation

$$\rho = \sum_i W_i c_i \tag{2.5}$$

boundary and initial conditions

$$\begin{cases} v(t,0) = v(t,L) = 0, \\ \dfrac{\partial}{\partial x}T(t,0) = \dfrac{\partial}{\partial x}T(t,L) = 0, \\ \dfrac{\partial}{\partial x}c_i(t,0) = \frac{\partial}{\partial x}c_i(t,L) = 0, \quad i = 1, \ldots, n_s, \\ v(0,x) = 0, \\ P(0,x) = 1 \text{ bar} \\ T(0,x) = 300 \text{ K} + (1200 \text{ K}) \exp\left[-\left(\dfrac{x}{l}\right)^2\right], \\ c_i(0,x) = X_i(0,x)\dfrac{P(0,x)}{R_0\, T(0,x)}, \quad i = 1, \ldots, n_s, \\ X_{\mathrm{H}_2} = \dfrac{2}{3}, \quad X_{\mathrm{O}_2} = \dfrac{1}{3}. \end{cases} \tag{2.6}$$

Here n_s – number of species, ρ – density of the mixture, T – temperature, P – thermodynamic pressure, R_0 – ideal gas constant, c_i – concentration of species i, X_i – molar fraction, h_i – specific molar enthalpy, j_i^d – molar diffusion flux, μ – shear viscosity of the mixture, λ – thermal conductivity of the mixture, $\dot{\omega}_i$ – chemical

source of species i, W_i – molar mass, Σ – flame folding factor. The thickness of the temperature profile l is chosen such that a minimal ignition energy is provided [24]. Note that equations (2.3) and (2.5) imply the conventional continuity equation,

$$\partial\rho/\partial t + \partial\rho u/\partial x = 0.$$

The effective coefficient of heat conductivity for gas mixture λ, shear viscosity coefficient μ and molar diffusion fluxes j_i^d are calculated with mixture average formulation [19, 41]. The latter was adjusted in order to insure mass conservation [8]:

$$j_i^d = j_i^{ma} - \frac{c_i}{\rho}\sum_k W_k j_k^{ma}, \tag{2.7}$$

where j_i^{ma} is the diffusion flux based on mixture average formulation.

The reaction mechanism of hydrogen-oxygen chemistry, containing 8 species and 38 elementary reactions, thermodynamical and transport data are applied from [32].

2.2. Numerical method

For integration of the system (2.1)–(2.6) a numerical method with time and space adaptation (Phlogia) has been recently developed. The code is based on pseudo-spectral method with interval matching [1]. Time integration (and discretisation) is equivalent to an implicit Runge-Kutta method [9] and space discretisation is derived from pseudo-spectral method with interval matching [1]. Spectral methods (SM) compared to fixed (low) order methods like Finite Volumes (FVM) or Finite Differences (FDM) require less grid points to reach the same accuracy [1]. In fact FVM and FDM can be seen as a special case of SM with fixed low polynomial order, *i.e.* when using power series of fixed order within one element (*e.g.* second order) and using interval indicators as test functions, leads to the classical finite volume method (see [1, 25] for more details).

In this study fixed second order approximation for time integration and variable order for space integration (between 4 and 16) were implemented. As for the accuracy discretization within the space and time is controlled with RTOL and ATOL parameters, which ensure the amplitude of truncated series of Chebyshev polynomials is below the specified level. Below, the details how the tolerance is calculated for a given spatial interval, time and component of the system state vector is presented.

The solution for the system state variables

$$\mathbf{u} = (u, T, c_1, c_2, \ldots, c_{n_s})^T$$

is split into blocks on intervals:

$$\begin{aligned} 0 = t_0 < t_1 < \cdots < t_{n_t} = \mathcal{T}, \\ 0 = x_0 < x_1 < \cdots < x_{n_x} = L. \end{aligned} \tag{2.8}$$

On each interval

$$I_{ij} := \begin{cases} t \in [t_{i-1}, t_i], \\ x \in [x_{j-1}, x_j], \end{cases} \tag{2.9}$$

let $U_k^{q_{ij}}(t,x)$ denote that polynomial of degree q_{ij} interpolates to a function $u_k(t,x)$ on the interval I_{ij} with a set of Chebyshev polynomials $\{\varphi_n(t,x)\}$:

$$U_k^{q_{ij}}(t,x) = u_k(t,x). \tag{2.10}$$

$U_k^{q_{ij}}(t,x)$ can be expanded without an error if an arbitrary large q_{ij} is chosen. The coefficients of this expansion:

$$U_k^{ij} = \sum_{l=0}^{q_{ij}} \widetilde{u}_{k,l}^{ij} \varphi_l \tag{2.11}$$

are calculated with pseudo-spectral method on the Gauss-Lobatto points [1].

Additionally, we link intervals with the following boundary conditions:

$$\begin{cases} U_k^{i,j}(t_{i-1},x) = U_k^{i-1,j}(t_{i-1},x), \\ U_k^{i,j}(t,x_{j-1}) = U_k^{i,j-1}(t,x_{j-1}), \\ U_k^{i,j}(t,x_j) = U_k^{i,j+1}(t,x_j), \qquad \forall\ k = 1,2,\ldots,n_{var}. \\ \frac{\partial}{\partial x} U_k^{i,j}(t,x_{j-1}) = \frac{\partial}{\partial x} U_k^{i,j-1}(t,x_{j-1}), \\ \frac{\partial}{\partial x} U_k^{i,j}(t,x_j) = \frac{\partial}{\partial x} U_k^{i,j+1}(t,x_j). \end{cases} \tag{2.12}$$

For practical consideration we choose degree of polynomial q_{ij} such that amplitude of truncated series does not exceed the specified tolerances:

$$\frac{\left|\widetilde{u}_{k,l}^{ij}\right|}{\max\limits_k \left\{ \max\limits_{(t,x)\in I_{ij}} \left|U_k^{ij}\right|,\ \mathrm{ATOL}_k \right\}} \le \mathrm{RTOL}_k,\ \forall\ l > q_{ij}. \tag{2.13}$$

The pseudo-spectral scheme of the system integration is shortly outlined as

1. The system solution on each integration time step t_i is split into intervals in the space. Within each of them it is approximated by a series of Chebyschev polynomials;
2. Then, the system solution is integrated and iterated simultaneously with interval adaptation procedure. The process stops when a specified tolerance of the Chebyschev polynomial representation is reached. Optimal distribution of the intervals and of the representation of the solution in each interval are found simultaneously. Note that the number of intervals and their size, as well as the order of approximating polynomials, are not constant over the integration in time as well as during the iteration within a particular time step;
3. Next, the system solution is extrapolated in time $t_i \to t_{i+1}$ and iterated again until the system is converged on the next time step etc.

The method is very close to the method of lines (see *e.g.* [38]). The use of Chebyschev polynomials and adaptive intervals allows us to speed up the integration time and to keep accuracy very high.

2.3. Validation

We validated our method with a well established code INSFLA [32, 33], which uses Lagrangian coordinates. INSFLA is also adaptive in time and space and has O(1) accuracy. The ignition problem was considered for $X_{H2} = 2/3$, $X_{O2} = 1/3$ and flame folding factor $\Sigma = 1$. The governing equations are described by equations (2.1)–(2.5), and boundary conditions are given by equation (2.6). The mixture was ignited with a hot spot width $l = 0.5$ mm and Temperature of $T = 1000$ K. During the ignition a shock wave is generated, which propagates ahead of the flame front and preheated the initial mixture from 300 K to 318 K and raised the pressure to 1.2 bar. In order to make quasi-incompressible code INSFLA comparable with the new method, we used adjusted initial values of temperature $T_0 = 318$ K and pressure $P = 1.2$ bar for INSFLA. It was observed that stationary profiles for temperature and concentration are optically indistinguishable. The relative difference is less than

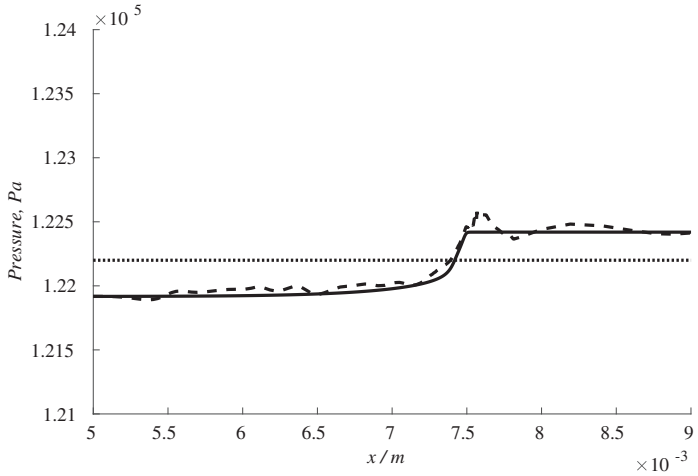

FIGURE 1. Comparison of stationary profile for pressure: dotted line – INSFLA, solid line – Phlogia RTOL $= 10^{-4}$, dashed line – Phlogia RTOL $= 10^{-3}$.

0.2 percent, which can be attributed to the neglected compressibility effects in INSFLA. The computed flame front velocity is also close: INSFLA is 87.1 m/s and Phlogia – 90.5 m/s.

In order to study the accuracy of the method the specified relative tolerance (RTOL), which provides an equivalent to the spacial resolution, is investigated. The influence of the RTOL on accuracy is best seen on the pressure profile. Figure 1 presents overlapped stationary profiles for pressure for INSFLA with 400 grid points and Phlogia with RTOL $= 10^{-4}$ and RTOL $= 10^{-3}$. ATOL was in all cases equal 10^{-8}. The profile with RTOL $= 10^{-3}$ have little oscillations near the flame front, which is particularly seen Figure 1. In fact these oscillations come from the spectral nature of the method and can be also observed by RTOL=10^{-4} but they become at least 10 times smaller (Fig. 2, *left*). In order to assess the error and accuracy the amplitude of solution oscillations, which arrives from the truncate series expansion, can be used as a measure for numerical error of the method. Thus, the relative error:

$$\epsilon_{rel} = \frac{\int_0^L \big(P(x) - P_{ref}(x)\big)\mathrm{d}x}{L \max\limits_x P(x)}, \tag{2.14}$$

shows the same characteristic behaviour as the oscillation amplitude. This is illustrated in Figure 2, where the relative error for pressure is compared to the amplitude of the oscillations and shown as function of the RTOL parameter. Here as a reference solution P_{ref} the solution with RTOL $= 10^{-5}$ has been employed.

3. The structure of the accelerated flames and of the DDT

3.1. Numerical implementation

The governing equations are described in Section 2, equations (2.1)–(2.5), and boundary conditions are given by equation (2.6). The ignition is initiated with the hot spot of a specified width. The initial profile (hot spot width l) is optimised in such a way that the outcome of the unsteady flame propagation is not influenced much by the presence of the hot spot specified at $x = 0$ (see Eq. (2.6)). In computations it is implemented by detailed study of the hot spot width l for different values of Σ such that minimising the chosen value of width of the hot spot by 5% leads to an ignition failure. The system is then integrated for different constant values of Σ and internal structure of the accelerating flame front is investigated (for details see [24]).

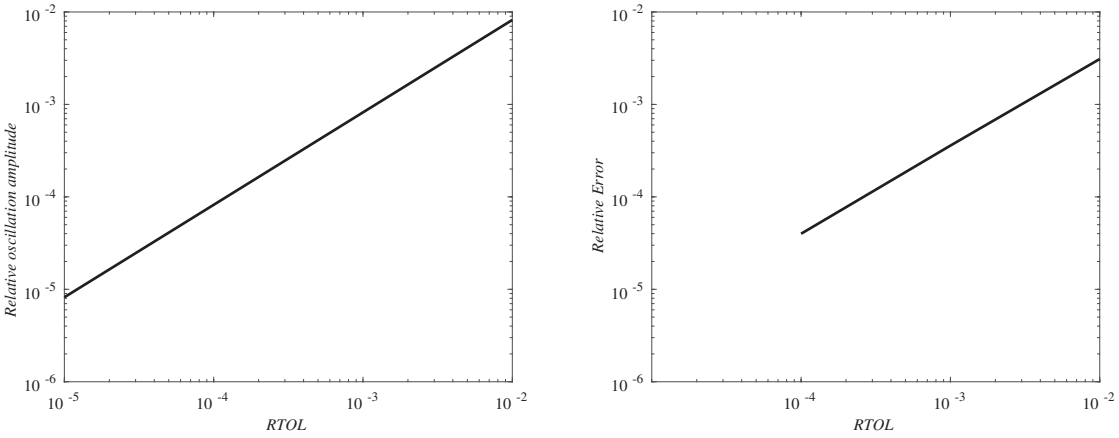

FIGURE 2. Relative amplitude of numerical oscillations (*left*) and relative error for pressure (*right*).

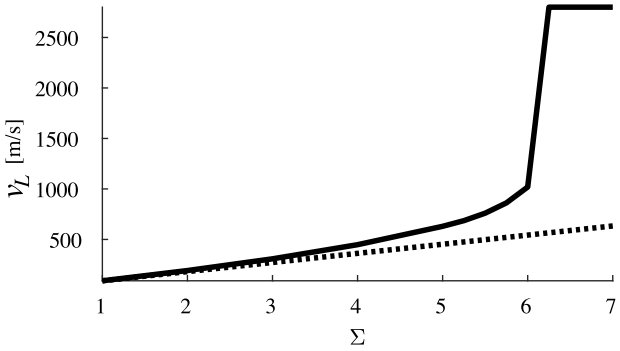

FIGURE 3. Flame speed as a function of Σ: solid line – actual flame speed, dotted line – extrapolated from laminar flame speed with $\Sigma = 1$.

As it was predicted and was shown in a number of works [16, 24] there is a critical value of Σ leading to very strong DDT, when an over-driven detonation is formed. Until this critical value is reached, flames with deflagration flame structure are observed with only a moderate pressure increase between the precursor shock and the flame front.

Figure 3 illustrates the flame front speed depending on Σ, where actual observed flame front speed is shown together with the one extrapolated from the normal deflagration velocity for $\Sigma = 1$ as $v_L(\Sigma) = v_L(1)\Sigma$. It can also be seen that starting from some value the actual flame velocity start deviating significantly and by reaching a critical value the flame front drastically accelerates leading to DDT.

By using generic algorithm for interval splitting, uniting and adaptive truncation of the approximating polynomial within the interval the new code can resolve the detonation wave structure with a high accuracy. A limited number of collocation points is used. The evolution of the pressure profile during the DDT can be seen in Figure 4 shows the resolved pressure profile at the moment of the DDT. The whole solution at this moment has 1114 collocation points on the interval $x = [0, 0.1]$ m, however, the relative amplitude of the truncated Chebyshev series does not exceed 10^{-4} on each sub-interval (see Eq. (2.13)). Required time for this computation accounted for 7 days on Intel i5-2310 CPU @2.90 GHz with 2 cores. The computation with $\mathrm{RTOL} = 10^{-3}$ requires twice as less points and twice as shorter CPU time but the results remain almost identical to $\mathrm{RTOL} = 10^{-4}$. The relative difference between these to computations is less than 10^{-3}.

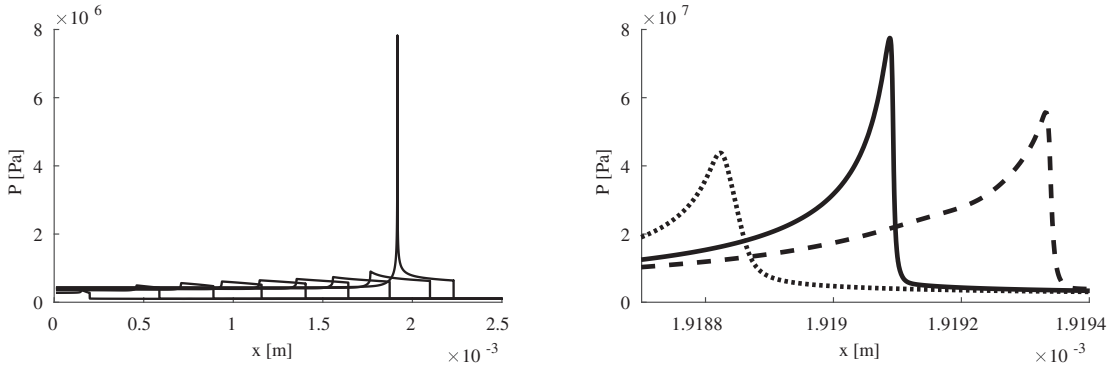

FIGURE 4. *On the left*: evolution of pressure profile for $\Sigma = 6.25$ before and at the DDT. *On the right*: zoom of the pressure profile for $\Sigma = 6.25$ at the DDT: solid line $t = 3.12378$ μs, dotted line $t = 3.12373$ μs, dashed line $t = 3.12382$ μs.

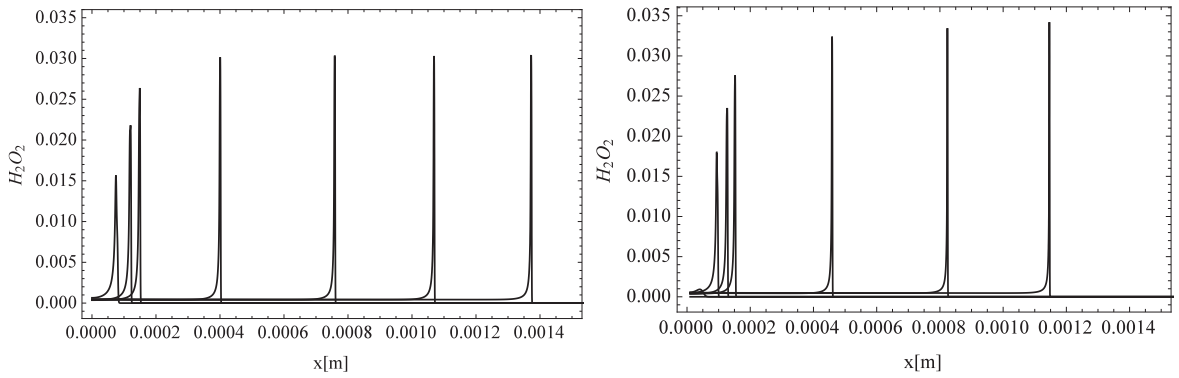

FIGURE 5. The radical profile of H_2O_2 specific mole numbers with the folding factor $\Sigma = 5.75$ over several instances of time (*left*). The radical profile of H_2O_2 specific mole number with the folding factor $\Sigma = 6.25$ over several instances of time (*right*).

3.2. Analysis of chemical kinetics in the DDT

In order to investigate the flame front structure we chose several values: one is shortly before the critical value $\Sigma = 5.75$ and the second one is slightly large than the critical value estimated by $\Sigma^* = 6$, namely, $\Sigma = 6.25$. All results for other values will be qualitatively very similar, thus, the chosen values are representative and used to compare and to study properties of the accelerating flames near the critical limit.

Now, we would like to understand how much the system thermo-kinetic states varies during the process of the flame acceleration. In order to investigate this, one needs to consider the evolution of the system equations (2.1)–(2.5) in the system state space, which in the case of detailed chemical kinetics is composed of species concentrations or can be also visualized by using specific mole numbers $\phi_i = Y_i/W_i = c_i/\rho\ ,\ i = 1, \ldots, n_s$ to avoid additional strong dependence on the pressure variation. Here Y_i is the mass fraction of species i.

First of all let us compare the evolution of the system in the initial stage right after the ignition, when a quasi-steady evolving profile of the flame front establishes. Figure 5 shows the profile evolution for minor species in the initial stage of the flame propagation. The profiles are shown for several but different instances in time for both $\Sigma = 5.75$ and $\Sigma = 6.25$. The profiles look very similar and follow during the initial stage after a short ignition period the same path even for minor species like H_2O_2 (see Fig. 6 as well). Figure 5 (*left and right*) shows the same trend of the system solution profiles during the ignition, deflagration and earlier flame

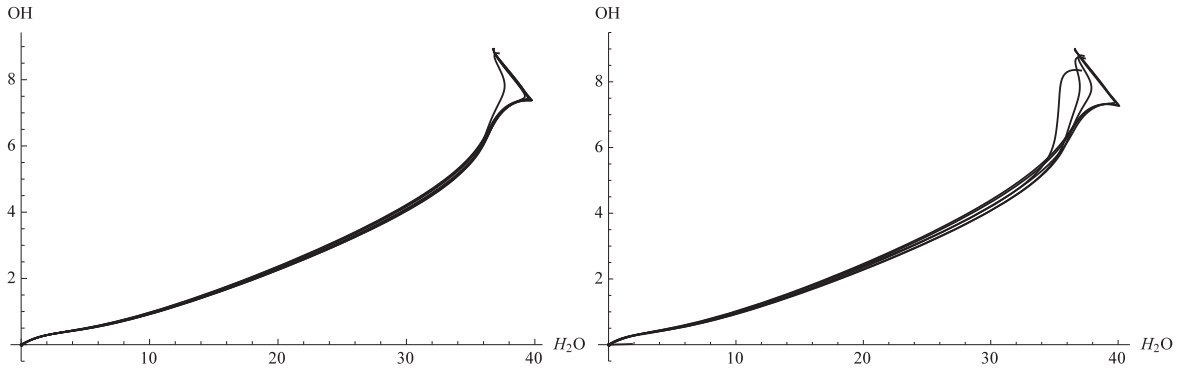

FIGURE 6. 2D projections of the profiles during DDT of the specific mole numbers of OH and H_2O for $\Sigma = 5.75$ (*left*) and for $\Sigma = 6.25$ (*right*).

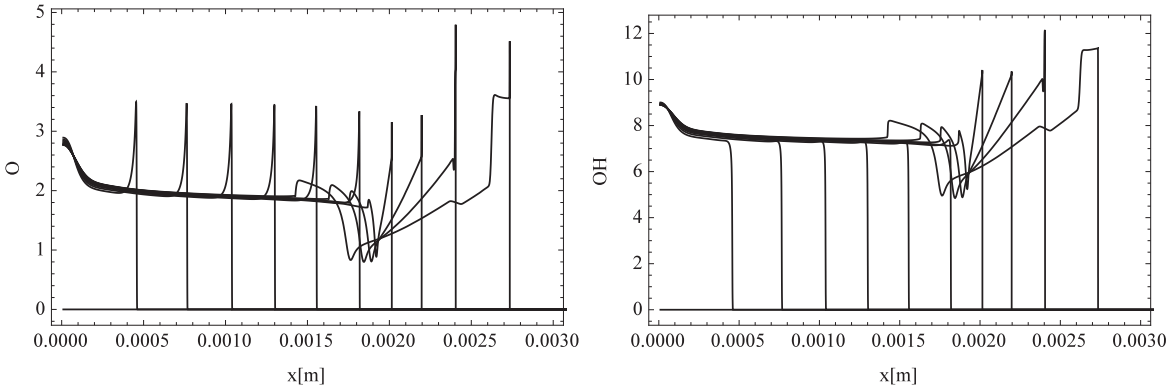

FIGURE 7. DDT process for O (*left*) and OH (*right*) radical species with $\Sigma = 6.25$.

acceleration stage stages. Note that they differ in time and in space but look very same in the projection of the state space (see *e.g.* Fig. 6).

Figure 6 shows the profile evolution in 2D projections to the specific mole numbers of OH and H_2O for both initial and later stages of the flame acceleration. The same profiles as in Figure 5 are shown on the plane (H_2O, OH) projection. It can be seen that at the initial stage the profiles follow the same path and converges to the same profile. Next, the stage of the flame acceleration and the transition are analysed in detail.

Figure 7 illustrates the species profiles during the DDT, where a significant variations of the specific mole numbers is observed. By further comparison of the system solution profiles (see Fig. 8) in this transient regime in the plane projection of the system thermo-chemical state space one can see how the quasi-stationary profile (lower solid line in Fig. 8) changes over time while the flame acceleration establishes. Both cases ($\Sigma = 5.75$ and $\Sigma = 6.25$), until this stage is reached, look very similar and remain identical but start to deviate strongly from the quasi-stationary profile for $\Sigma = 5.75$ as the DDT is approached. Finally, after the DDT (shown by dashed lines) a new stationary profile establishes (shown by the upper solid line in Fig. 8).

Complications of chemical kinetics becomes more transparent in a 3D projection. Figure 9 shows projections of specific mole numbers of (H_2O, H_2, OH) and (O, H, OH) space for the cases $\Sigma = 5.75$ and $\Sigma = 6.25$ during the transient process. The states that belong to solution profiles during the deflagration stage are marked by red. The difference in other radical projection between $\Sigma = 5.75$ and $\Sigma = 6.25$ is also significant, however it is more pronounced for O, H and OH radicals. One can see that for both parameters, system profiles are the same and lay on one dimensional path in the state space. Later on during the stages of DDT the states scatter and have

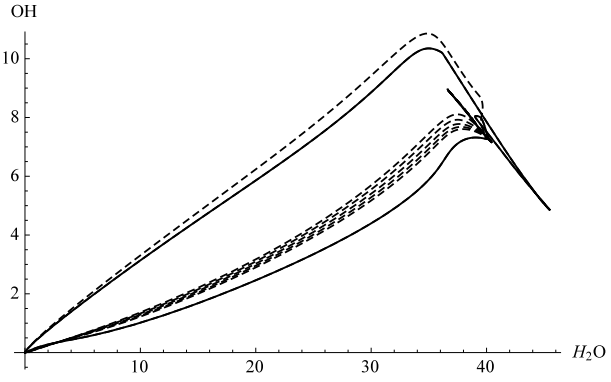

FIGURE 8. 2D projections of the profiles of the specific mole numbers of OH and H_2O with the folding factor $\Sigma = 6.25$: dashed lines – initiation of detonation, solid line – steady propagation.

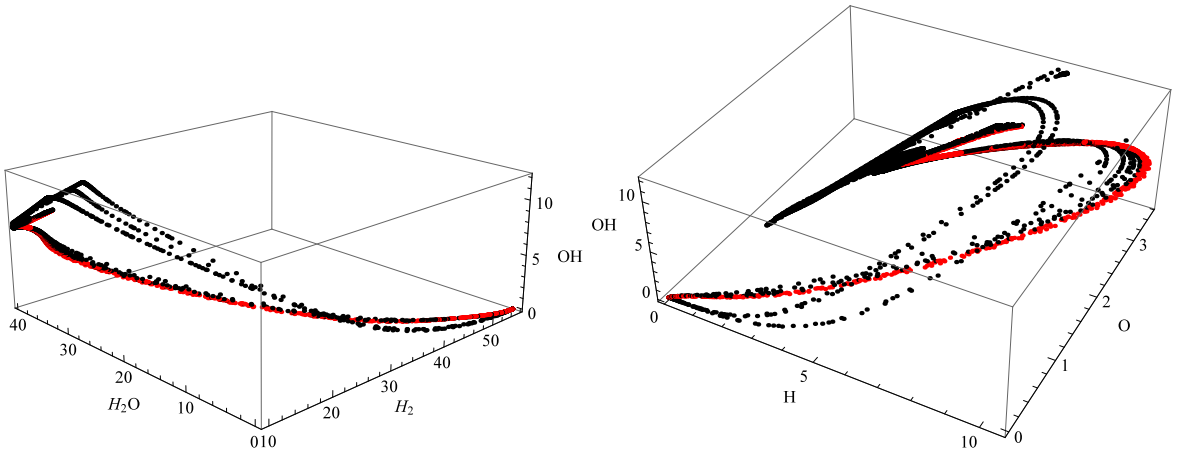

FIGURE 9. *On the left*: 3D projections of the profiles of the specific mole numbers of H_2O, H_2 and OH. *On the right*: profiles of the specific mole numbers of O, H and OH. red points – deflagration with $\Sigma = 5.75$, black points – DDT with $\Sigma = 6.25$.

multidimensional structure. Furthermore after the DDT the solution profile becomes one dimensional again but the solution follows now a different path in the stat space (Fig. 6). Although initial and final solutions are one dimensional in the state space, they are different and during the transition even in three dimensional projection we observe a cloud of states. This means that even a two dimensional description might be not enough.

Finally, in order to illustrate what kind of analysis and information can be gained from the system integration data a local version of the criteria proposed in [22, 23] provides an additional tool for comparison and validation. Accordingly, Figure 10 shows evolution of the speed of the flame front, the sound speed at the maximum of the pressure and the sound speed in products. The data of the numerical computations are now used to delineate the flame front at the position of the maximal gradient of the OH and calculate the speed of the reaction front during the flame acceleration stage. At the same time, we compare it with the sound velocity in the product and with the sound velocity at the entrance to the flame front indicated by the maximum of the pressure.

As predicted by the global criteria [22] the DDT occurs when the flame accelerates faster (as function of the pressure) than the sound velocity in fresh compressed mixture at the point where the front speed reaches the velocity in the products shown in Figure 10 by the dotted line. One can see that in the first scenario with $\Sigma = 5.75$ shown in Figure 10 after the initial ignition period all three characteristics remain almost constant.

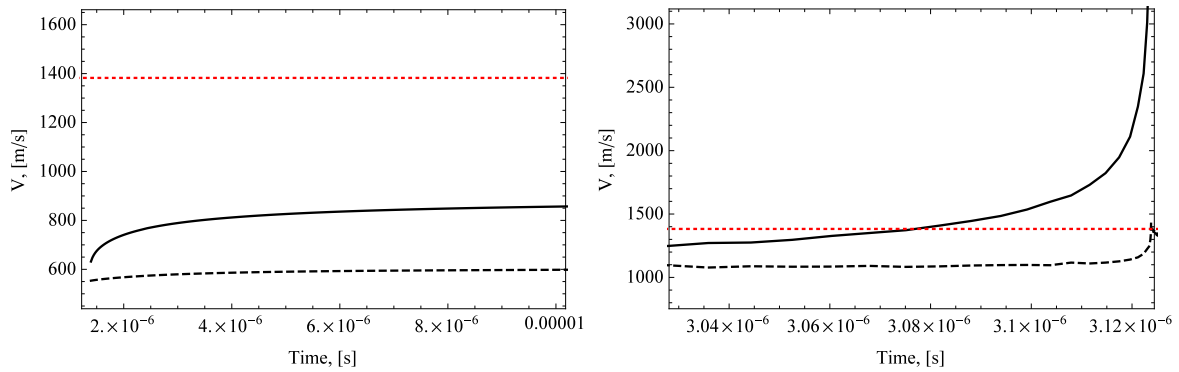

FIGURE 10. Comparison of critical velocities for $\Sigma = 5.75$ (*left*) and $\Sigma = 6.25$ (*right*). Solid line – flame speed, dashed line – sound velocity at the position of maximal pressure, dotted line – sound velocity in the products.

Thus, the quasi-steady deflagration regime is reached. However, in the second scenario (Fig. 10 on the right) the flame front accelerates further in a very short time. During the acceleration the sound velocity of the Neumann state (right behind the shock, where the pressure reaches maximal values) grows very slowly and when the front velocity reaches the sound velocity in the products rapid flame front acceleration is observed with subsequent DDT.

4. Conclusions

The Σ model was implemented to study the flame acceleration and the DDT phenomenon. The flame ignites at $x = 0$ and propagates in a stoichiometric hydrogen/oxygen mixture in the half plane $x > 0$. A novel pseudo-spectral method was presented and employed for parametric studies. It allows to treat the DDT at all scales and it can be used for integration of the system with detailed chemical kinetics and mixture averaged diffusion models.

By using initial conditions that guaranties a mild ignition flame acceleration stages are captured in all details. The suggested scheme can be used to gain the detailed flame structure, which allows us to perform an analysis of the DDT in the system thermochemical state space.

It was shown that the system thermo-chemical state space during the DDT has very complicated and high dimensional structure if compared to the deflagration regime of the flame propagation. This means that in order to model the DDT quantitatively multiple-stage chemical reaction mechanisms have to be employed. Additionally, the analysis of the fine structure of the flame acceleration was provided to check and validate an analog of the global criteria suggested recently. Indeed, it was observed for the critical flame folding parameter, the local speed of the flame front at the transition stage, by reaching the sound velocity in the products, accelerates much faster than the sound velocity at the point of maximal pressure. This confirms indirectly the suggested global criterion for DDT.

References

[1] J.P Boyd, Chebyshev and Fourier spectral methods. Courier Corporation (2001).
[2] I. Brailovskya and G. Sivashinsky, Hydraulic resistance and multiplicity of detonation regimes. *Combust. Flame* **122** (2000) 130–138.
[3] V. Bychkov, D. Valiev, V. Akkerman and C.K. Law, Gas compression moderates flame acceleration in deflagration-to-detonation transition. *Combust. Sci. Technol.* **184** (2012) 1066–1079.
[4] V. Bychkov, D. Valiev and L.-E. Eriksson, Physical mechanism of ultrafast flame acceleration. *Phys. Rev. Lett.* **101** (2008) 164501.
[5] V. Bykov, I. Goldfarb, V. Gol'dshtein, L. Kagan and G. Sivashinsky, Effects of hydraulic resistance and heat losses on detonability and flammability limits. *Combust. Theory Model.* **8** (2004) 413–424.

[6] P. Clavin, Dynamics of combustion fronts in premixed gases: from flames to detonations. *Proc. Combust. Inst.* **28** (2000) 569–585.

[7] P. Clavin and L. He, Acoustic effects in the nonlinear oscillations of planar detonations. *Phys. Rev. E* **53** (1996) 4778.

[8] T.P. Coffee and J.M. Heimerl, Transport algorithms for premixed, laminar steady-state flames. *Combust. Flame* **43** (1981) 273–289.

[9] M. Delfour, W. Hager and F. Trochu, Discontinuous galerkin methods for ordinary differential equations. *Math. Comput.* **36** (1981) 455–473.

[10] B. Deshaies and G. Joulin, Flame-speed sensitivity to temperature changes and the deflagration-to-detonation transition. *Combust. Flame* **77** (1989) 201–212.

[11] H. Freiwald and H.W. Koch, Spherical detonations of acetylene-oxygen-nitrogen mixtures as a function of nature and strength of initiation. In Vol. 9 of *Symposium (International) on Combustion*. Elsevier (1963) 275–281.

[12] L. He, Theoretical determination of the critical conditions for the direct initiation of detonations in hydrogen–oxygen mixtures. *Combust. Flame* **104** (1996) 401–418.

[13] M.F. Ivanov, A.D. Kiverin and M.A. Liberman, Hydrogen–oxygen flame acceleration and transition to detonation in channels with no-slip walls for a detailed chemical reaction model. *Phys. Rev. E* **83** (2011) 056313.

[14] L. Kagan and G. Sivashinsky, Deflagration-to-detonation transition in narrow channels: hydraulic resistance versus flame folding. *Combust. Theory Model.* **20** (2016) 798–811.

[15] L. Kagan and G. Sivashinsky, Parametric transition from deflagration to detonation: runaway of fast flames. *Proc. Combust. Inst.* **36** (2017) 2709–2715.

[16] L. Kagan and G. Sivashinsky, Transition to detonation of an expanding spherical flame. *Combust. Flame* **175** (2017) 307–311.

[17] K. Kailasanath, Recent developments in the research on pulse detonation engines. *AIAA J.* **41** (2003) 145–159.

[18] V. Kamenskihs, H.D. Ng and J.H.S. Lee, Measurement of critical energy for direct initiation of spherical detonations in stoichiometric high-pressure H_2–O_2 mixtures. *Combust. Flame* **157** (2010) 1795–1799.

[19] R.J. Kee, M.E. Coltrin and P. Glarborg, Chemically reacting flow: theory and practice. John Wiley & Sons (2005).

[20] A.M. Khokhlov, E.S. Oran and J. Craig Wheeler, A theory of deflagration-to-detonation transition in unconfined flames. *Combust. Flame* **108** (1997) 503–517.

[21] A.D. Kiverin, I.S. Yakovenko and M.F. Ivanov, On the mechanisms and criteria of deflagration-to-detonation transition in gases. *J. Phys. Conf. Ser.* **754** (2016) 0520026.

[22] A.D. Kiverin, I.S. Yakovenko and M.F. Ivanov, On the structure and stability of supersonic hydrogen flames in channels. *Int. J. Hydrogen Energy* **41** (2016) 22465–22478.

[23] A.D. Kiverin, D.R. Kassoy, M.F. Ivanov and M.A. Liberman, Mechanisms of ignition by transient energy deposition: regimes of combustion wave propagation. *Phys. Rev. E* **87** (2013) 033015.

[24] A. Koksharov, V. Bykov, L. Kagan and G. Sivashinsky, Deflagration-to-detonation transition in an unconfined space. *Combust. Flame* (2018).

[25] A. Koksharov, C. Yu, V. Bykov, U. Maas, M. Pfeifle and M. Olzmann, Quasi-spectral method for the solution of the master equation for unimolecular reaction systems. *Inte. J. Chem. Kinet.* **50** (2018) 357–369.

[26] M. Kuznetsov and J. Grune, Experiments on flame propagation regimes in a thin layer geometry. In *Proc. of the 26th ICDERS* (2017).

[27] M. Kuznetsov, A. Lelyakin, V. Alekseev and I. Matsukov, Detonation transition in relatively short tubes. In *30th International Symposium on Shock Waves 1*. Springer (2017) 481–485.

[28] M. Kuznetsov, M. Liberman and I. Matsukov, Experimental study of the preheat zone formation and deflagration to detonation transition. *Combust. Sci. Technol.* **182** (2010) 1628–1644.

[29] M. Kuznetsov, R. Redlinger, W. Breitung, J. Grune, A. Friedrich and N. Ichikawa, Laminar burning velocities of hydrogen-oxygen-steam mixtures at elevated temperatures and pressures. *Proc. Combust. Inst.* **33** (2011) 895–903.

[30] M. Lam, D. Tillie, T. Leaver and B. McFadden, Pulse detonation engine technology: an overview. The University of British Columbia (2004).

[31] J.H.S. Lee, The detonation phenomenon, Vol. 2. Cambridge University Press, Cambridge (2008).

[32] U. Maas and J. Warnatz, Ignition processes in hydrogen oxygen mixtures. *Combust. Flame* **74** (1988) 53–69.

[33] U. Maas, *Mathematische Modellierung instationärer Verbrennungsprozesse unter Verwendung detaillierter Reaktionsmechanismen*. Ph. D. thesis, Ruprecht-Karls-Universität Heidelberg (1988).

[34] M.A. Nettleton, Gaseous detonations: their nature, effects and control. Springer Science & Business Media (2012).

[35] E.S. Oran and V.N. Gamezo, Origins of the deflagration-to-detonation transition in gas-phase combustion. *Combust. Flame* **148** (2007) 4–47.

[36] A. Palm-Leis and R.A. Strehlow, On the propagation of turbulent flames. *Combust. Flame* **13** (1969) 111–129.

[37] A.Y. Poludnenko, T.A. Gardiner and E.S. Oran, Spontaneous transition of turbulent flames to detonations in unconfined media. *Phys. Rev. Lett.* **107** (2011) 054501.

[38] A. Quarteroni and S. Quarteroni, Numerical models for differential problems, Vol. 2. Springer (2009).

[39] H. Shen and M. Parsani, The role of multidimensional instabilities in direct initiation of gaseous detonations in free space. *J. Fluid Mech.* **813** (2017).

[40] D. Valiev, V. Bychkov, V. Akkerman, C.K. Law and L.-E. Eriksson, Flame acceleration in channels with obstacles in the deflagration-to-detonation transition. *Combust. Flame* **157** (2010) 1012–1021.

[41] J. Warnatz, U. Maas, R.W. Dibble and J. Warnatz, Combustion, Vol. 3. Springer (1996).

[42] F.A. Williams, Combustion Theory. Cummings Publ. Co (1985).
[43] H. Xiao, R.W. Houim and E.S. Oran, Formation and evolution of distorted tulip flames. *Combust. Flame* **162** (2015) 4084–4101.
[44] Y.B. Zeldovich, V.B. Librovich, G.M. Makhviladze and GIi Sivashinsky, On the development of detonation in a non-uniformly preheated gas. *Astron. Acta* **15** (1970) 313–321.
[45] Y.B. Zeldovich and A.I. Rozlovskii, On the onset of unstable normal burning: transition of a spherical flame to detonation. *Dokl. Akad. Nauk SSSR* **57** (1947) 365–368.
[46] X. Zhen, Y. Wang, S. Xu, Y. Zhu, C. Tao, T. Xu and M. Song, The engine knock analysis – an overview. *Appl. Energy* **92** (2012) 628–636.